ANALYSIS OF THE CMB POLARIZATION MAPS IN THE FRAME OF THE GENERALIZED PARETO DISTRIBUTION AND COMPLETE CORRELATIONS

Raoul R. NIGMATULLIN[1], Dumitru BALEANU[2 3], Ovidiu TINTAREANU-MIRCEA[3 *]

In this paper, the authors use the generalized Pareto distribution (GPD) to analyze the Stokes (Q) and (U) CMB polarization anisotropies, as measured by the ESA's Planck space mission. The analyzed dataset is one of the twelve HEALPix regions, obtained using the SMICA pipeline, one of the 4 methods that produced the Planck CMB maps cleaned of foreground noise. The CMB polarization random fluctuations can be "read" accurately by the generalized Pareto distributions. These distributions representing a linear combination of power-law functions turned out to be effective for describing the distributions having clearly expressed long tails. The arguments of application of these power-law distributions are given inside the paper.

Keywords: Generalized Pareto distribution, CMB, Planck satellite.

1. Introduction

The Cosmic Microwave Background (CMB), is a blackbody radiation emitted at the time the Universe became transparent due to recombination of electrons and nuclei that formed first neutral primordial atoms. The CMB is remarkably homogeneous and isotropic, its temperature at current epoch being 2.72548±0.00057 K [1], nevertheless have been detected small fluctuations of this temperature at a level of 10^{-5} from different directions, called anisotropies. They correspond to variations in the density of matter at the time that the CMB formed and the exact anisotropy pattern depends on cosmological parameters. By varying all the different parameters, it is possible to create a cosmological model with an impressively good fit to the observed data.

Besides the temperature anisotropies, CMB data have also polarization anisotropies originating from scattering of the primordial photons having a non-

[1] Kazan National Research Technical University named after A.N. Tupolev, Radioelectronics and Informative Measurements Technics department, renigmat@gmail.com
[2] Department of Computer Science and Mathematics, Lebanese American University, Beirut, Lebanon, dumitru.baleanu@lau.edu.lb
[3]* Institute of Space Science – INFLPR subsidiary, Magurele-Bucharest, Romania (Corresponding author)

zero quadrupole moment very near to the surface of last scattering [2, 3]. Studying the fluctuations in the CMB polarization unveils crucial information about the early universe, including the generation of cosmic structure, the presence of primordial gravitational waves, and fundamental cosmological parameters. The CMB polarization can be decomposed into a zero-curl E-mode and a zero-divergence B-mode [4, 5]. While the E-mode mainly originates in scalar matter density perturbations, the B-mode are mainly generated by primordial gravitational waves (tensor perturbations) or by gravitational lensing. The vector perturbations, due to matter vorticity upon recombination, have no measurable imprint on the CMB polarization in standard cosmological models. The Planck mission did not measure the E and B modes, but the Stokes Q (the difference in intensities between "horizontal" and "vertical" linearly polarized components) and U (the difference in intensities between linearly polarized components oriented at +45° and −45°) parameters of the linearly polarized CMB. The E and B modes are derived by a spin-2 spherical harmonic decomposition on the celestial sphere, separating the gradient-like (E-mode) and curl-like (B-mode) patterns based on their parity. The distinct influence of scalar/vector/tensor perturbations is present only relative to the E and B modes, not to the Stokes parameters Q and U.

In this study, we analyzed the Stokes Q and U CMB polarization data, obtained by the SMICA [6] pipeline. In order to describe the CMB polarization fluctuations we apply the generalized Pareto distribution (GPD) representing a linear combination of power-law exponents (see expressions (2) and (4)). Why the GPD(s) were turned out to be effective in descriptions of random fluctuations? Actually, two arguments should be taken in account. The first argument is related to envelopes behavior of the F-transform of the low-frequency noise having power-law behavior. Logically, from this observation it follows that envelopes of the fluctuations should have power-law behavior too. The second argument is associated with the power-law behavior of the "long-heavy tails" of many distributions that are degenerated in power-law behavior clearly expressed in ergodic behavior of the ranged amplitudes of the corresponding fluctuations. In this paper we combine these two observations and present them in compact form that can be applied for descriptions of fluctuations of the random sequences (CMB data) not having clearly expressed trend. The rest of the paper is organized as follows. In Section 2 we describe the analyzed dataset. In Section 3 we describe the data processing procedure and present the results of our method. In the final Section 4 we summarize and discuss our results.

2. Data description

Although Planck measured the CMB polarization anisotropies at nine frequencies from 30 to 857 GHz, there are also some combined maps

(COMMANDER, NILC, SEVEM and SMICA) accounting for some linear combinations of frequency maps. We have considered the SMICA CMB maps [6] presented in the form of 1D arrays with 50,331,648 elements, each element corresponding to a given set of sky coordinates. This corresponds to HEALPix (Hierarchical Equal Area isoLatitude Pixelization) [7] nested ordering format with Nside = 2048 (order N=11). We cut from these maps the primarily pixel "0" (1/12 part of full sky) and rearrange the 1D array in 2D arrays such that adjacent pixels in the matrix are also adjacent on the sky.

3. Data processing procedure

For the fitting purposes the authors of this paper obtained two square matrices, Q and U, referring to Stokes Q and U polarizations. Each matrix has N (N=2048 rows) × M (M=2048 columns). How to receive adequate and reliable reduced set of parameters characterizing these set of big data from the general point of view? For achieving this aim, one can propose the following processing procedure. It can be divided on some basic steps that have general character and can be applied for a wide class of different fluctuations. In the previous paper [8] the authors analyzed temperature anizotropy. In present paper one can consider the Stokes Q and U polarization anizotropy matrices.

S1. One can start evaluation of the number of the roots crossing the "zero" (mean value) line. We noticed that distribution of the roots (crossing zero line) follows approximately to the straight line $R(k)=Ak + B$ (k=0,1…,K), where k is the number of the current root, A and B define the slope and the corresponding intercept, K defines the total number of roots. Based on this property one can calculate the number of the roots and mean dimensionless frequency <ω> and phase Φ from the obvious relationship (as it is well-known that trigonometric functions exactly follow to the *linear* distribution of their roots)

$$cos(\langle\omega\rangle \cdot R_k - \Phi) = 0, or\ \langle\omega\rangle \cdot R_k - \Phi = \frac{\pi}{2} + \pi \cdot k,$$
$$\langle\omega\rangle = \frac{\pi}{A}, \Phi = \langle\omega\rangle B - \frac{\pi}{2} \quad (1)$$

Therefore, 4 basic parameters as K, < ω >, A and B can characterize the intensity of fluctuations. They are shown inside the Fig. 1 together with the plots of the roots distribution for (Q) and (U) matrices.

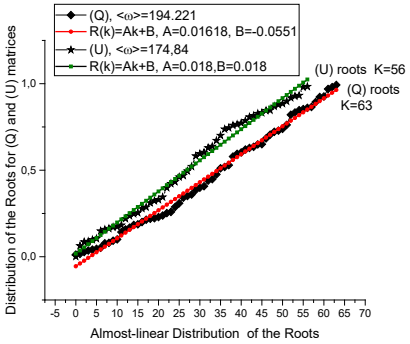

Fig. 1. Quasi-linear distribution of the roots corresponding to (Q) and (U) matrices

S2. The second step in the processing of random fluctuations is the creation of the so-called confidence tube (CT). If from each column of the initial matrix we choose only three points (maximal, mean and the minimal values, accordingly) then propagating this procedure over all columns we obtain three distributions Tup(*m*) (max. values), Tmn(*m*) (mean values) and Tmin(*m*) (minimal values), where index *m*=0,1,2,…, *M* (*M*=2047) defines the number of the current column. These three distributions for (Q) and (U) data, accordingly, are shown in Figs. 2 (a,b).

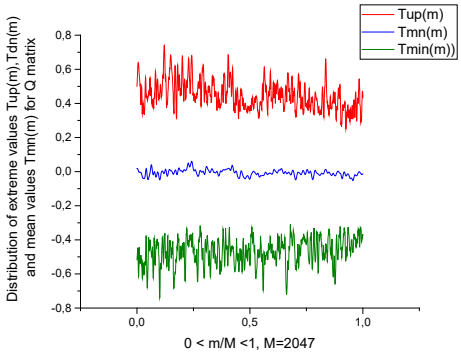

Fig. 2(a). Distribution of the extreme values for the matrix (Q). Mean values for this matrix is given below because of the different scales.

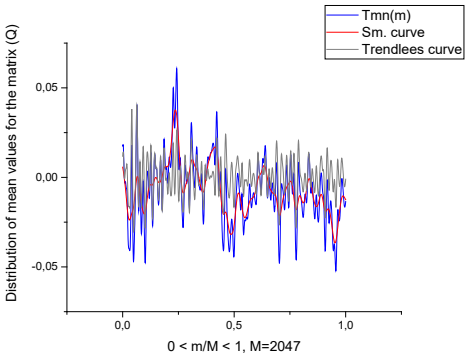

Fig. 2(b). The plots demonstrate the distribution of Tmn(m) for the matrix (Q) with clearly expressed oscillations (blue color). Distribution given in red lines refers to the smoothed curve associated with trend. After its substruction one can obtain the trendless gray curve.

We should notice that these distributions are invariant relatively to all data points permutations located inside each column. Another CT for (U) data has a sense to reproduce also. They are shown in Figs. 3 (a,b).

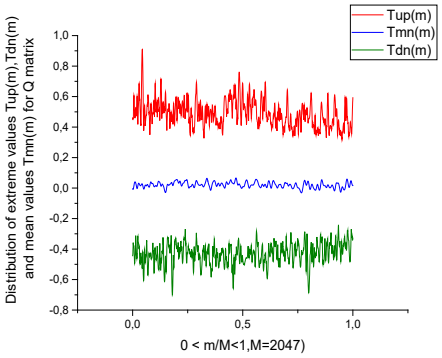

Fig. 3(a). Distribution of the extreme values for the matrix (U). Mean values for this matrix is given below because of the different of scales.

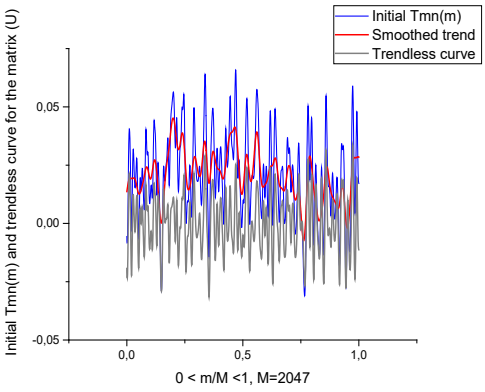

Fig. 3(b). The plots demonstrate the distributions of Tmn(m) with clearly expressed oscillations (shown in blue color). Distribution given in red lines refers to the smoothed curve associated with trend. After its substruction one can obtain the trendless curve given in grey color below.

We should notice that distributions of the mean values Tmn(m) demonstrate clearly the hidden oscillations and these random "vibrations" can be associated with possible anisotropy of the analyzed matrices (Q) and (U).

S3. The next step of the proposed treatment is the fitting of the sequences of the range amplitudes (SRAs) bisected on two parts (forming positive and negative ordered fluctuation amplitudes (branches), accordingly. Being summarized (or integrated by the trapezoid method) these branches form distributions of the cumulative or total value fluctuations as well. The verification of data with the help of the ECs method [9] shows that these envelopes are described by the generalized Pareto distributions (GPD). The GPD is determined by expression

$$Pr_P(t) = \sum_{p=0}^{P-1} A_p t^{\nu_p} \qquad (2)$$

where $Pr_P(t)$ defines the linear combination of power-law terms or some polynomial.

Any reader may ask why the authors chose expression (2) for the fitting purposes? Part of the arguments was given in the previous paper [8] based on the self-similarity principle. In this paper we want to justify selection (2) from the (non)ergodicity principle. If we take the pair of trendless sequences (representing a "noise") and calculate the pair correlation function based on the well-known formula

$$Cr_m(y1, y2) = \frac{1}{2\cdot(N-m)} \sum_{j=1}^{N-m} \left(y1_j y2_{j+m} + y1_{j+m} y2_j\right), m = 0,1,..N-1 \qquad (3)$$

then we obtain the correlation "noise" which keeps its non-equilibrium state (nonergodicity) for all values of the correlation parameter m. The ordering of this

nonergodicity expressed in the form of the corresponding sequences of the ranged amplitudes (SRA) that transform initial sequence as pseudo-equilibrium or ergodic. Therefore, the analysis of the SRA which admits the quantitative parametrization has an essential importance. We should add also the following fact. In long-term studies of low-frequency (LF) "noise" related to various phenomena, it has been noted that the behavior of LF envelopes in the frequency domain has a power-law behavior expressed approximately in the form $A(f) \cong af^{-\beta_f}$. It is assumed that the power-law exponent β_f is localized in the interval [0,1], although there are cases when this parameter goes beyond the boundaries of this interval. It is clear that such an estimate is an approximation, but nevertheless, this fact means that the behavior of correlations in the time domain follows to the power-law behavior. Based on this real information, one can assume that the behavior of the SRA, preliminarily splintered into positive and negative branches can be fitted accurately by the following functions

$$Pr_3(t) = \begin{cases} \sum_{p=0}^{2} A_p t^{\nu_p}, Im(\nu_p) = 0 \\ A_0 t^{\nu_0} + A_1 t^{Re(\nu_1)} cos(|Im(\nu_1)| ln(t)) + A_2 t^{Re(\nu_1)} sin(|Im(\nu_1)| ln(t)) \end{cases} \quad (4a)$$

$$Pr_2(t) = \begin{cases} \sum_{p=0}^{1} A_p t^{\nu_p}, Im(\nu_p) = 0 \\ A_0 t^{Re(\nu_0)} cos(|Im(\nu_0)| ln(t)) + A_1 t^{Re(\nu_0)} sin(|Im(\nu_0)| ln(t)) \end{cases} \quad (4b)$$

The verification on real data indicates that for practical purposes (for achieving the value of the relative error less than 5%) it is sufficient to choose P=3 for the fitting of positive and negative branches, correspondingly. For smoother curves as integral/cumulative curves we choose only two terms (P=2). Below, we define these fitting functions as the generalized Pareto distributions (GPD).

These GPDs (4) will be used for the fitting of the positive (2) and negative branches (2) for CT(s) distributions, shown on the Figs. 2 and 3, correspondingly. We should stress here a specific "universality" of the functions (4). For more deep analytical purposes one can apply these fitting functions directly for each selected column of the chosen matrix (Q) or (U). The authors are not able to demonstrate the fit of all columns (M=2048! – it is too much), because the excess information that will be contained in these figures and tables will exceed considerably the page limitations of any scientific journal. Therefore, the authors are concentrated on the fitting of the CTs distributions that are obtained from initial (Q,U) matrices. Below, it is convenient to work with sizeless data. Therefore, the CTs distributions will be normalized on their range as

$$DT(m) = \frac{T(m)}{Range(T)}, 0 < DT(m) < 1, \quad (5)$$

$$Range(T) = max(T) - min(T) > 0.$$

As it has been mentioned above nonlinear power-law exponents will be found by the ECs method [9], allowing the reduction of the nonlinear fitting procedure to the linear least square method (LLSM).

The Figs. 4 (a, b, c) demonstrate the normalized SRA that are prepared for the fitting purposes.

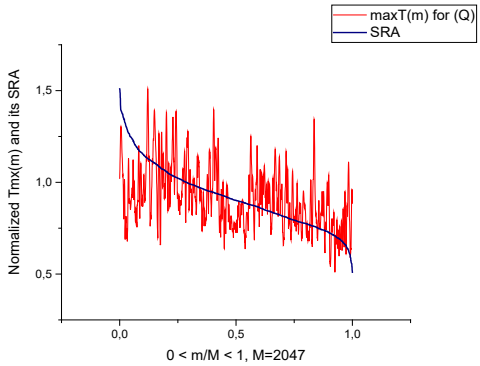

Fig. 4(a). The normalized "noise" sequence associated with Tup(m) belonging to (Q) matrix. The SRA given by solid black line is expressed clearly. After bisection of this curve on the positive and negative parts we will apply the fitting expressions (4a). The fit of these bisected envelopes is shown below.

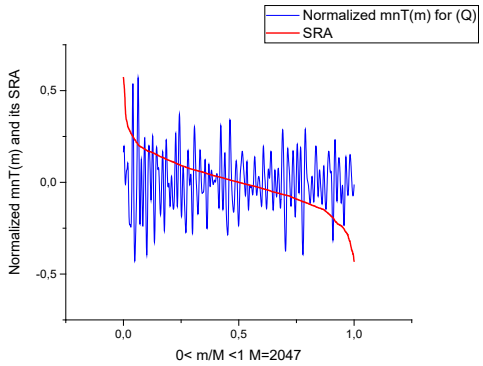

Fig. 4(b). The normalized "noise" sequence associated with Tmn(m) belonging to (Q) matrix. The SRA given by solid red line is expressed clearly. After bisection of this curve on the positive and negative parts we will apply the fitting expressions (4a). The fit of these bisected envelopes is shown below.

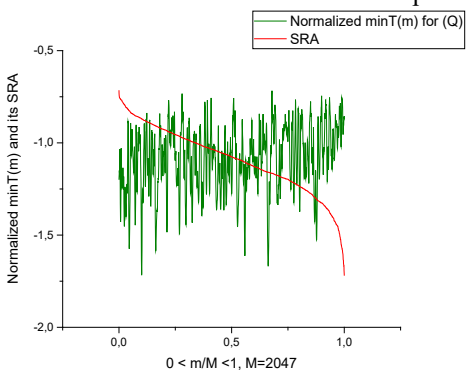

Fig. 4(c). The normalized "noise" sequence associated with the normalized Tmin(m) belonging to (Q) matrix. The SRA given by solid red line is expressed clearly. After bisection of this curve on the positive and negative parts we will apply the fitting exp

The results of the application of the ECs method are shown in Figs. 5 (a, b, c) (for initial envelopes), and 6 (a, b, c) (for integral envelopes), correspondingly. We should give these figures independently from each other because the length of each distribution is different. Other two (for the matrix U) types of fluctuations are considered in the similar manner and, therefore these figures are not shown.

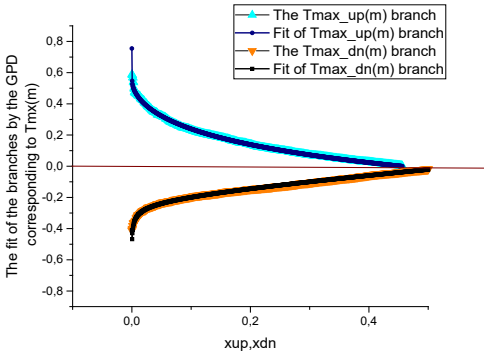

Fig. 5(a). The fit of the envelopes by the GPD corresponding to Tmax(m). All fitting parameters corresponding to the GPD are collected in Table 1.

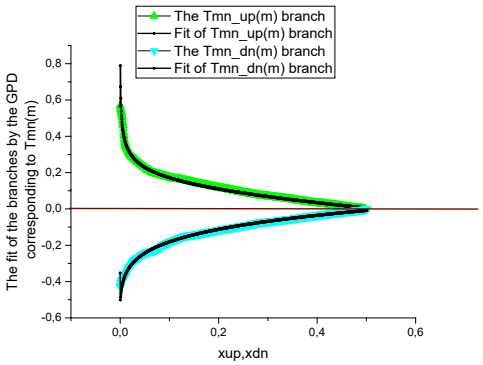

Fig. 5(b). The fit of the envelopes by the GPD corresponding to Tmn(m). All fitting parameters are collected in Table 1.

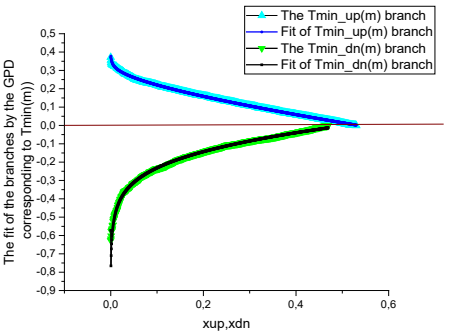

Fig. 5(c). The fit of the envelopes by the GPD corresponding to integral Tmin(m). Fitting parameters are collected in Table 1.

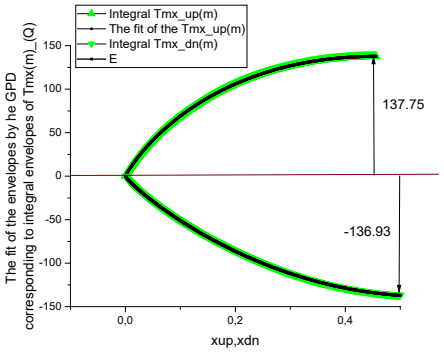

Fig. 6(a). The fit of the envelopes by the GPD corresponding to the integral Tmax(m). Fitting parameters are collected in Table 2.

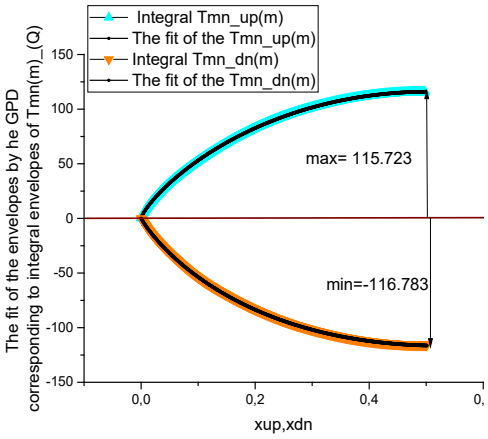

Fig. 6(b). The fit of the envelopes by the GPD corresponding to the integral Tmn(m). Fitting parameters are collected in Table 2.

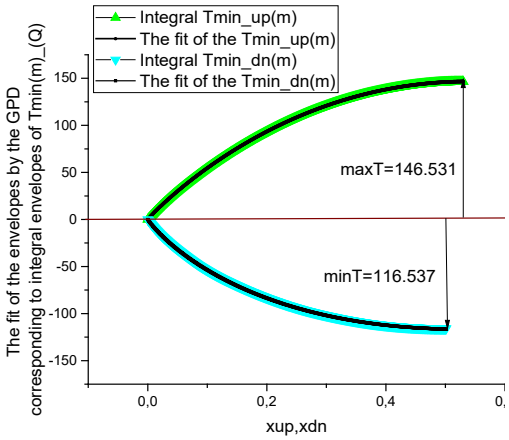

Fig. 6(c). The fit of the envelopes by the GPD corresponding to the integral Tmin(m). Fitting parameters are collected in Table 2.

All necessary fitting parameters figuring in expressions (3a) and (3b) for all Q, U data are collected in Tables 1, 2 (for (Q) data) and Tables 3, 4 (for (U) data).

Table 1.

The set of the fitting parameters corresponding to the GPD in accordance with expression (4a) realized for the matrix (Q)

T(m)	ν_0	*Re*(ν_1)	/*Im*(ν_1)/	ν_2	A_0	A_1	A_2	*RelErr(%)*
Tmx_up	-1.4072	-0.2525	0.00000	0.7585	-0.00380	0.1192	-0.2283	6.71922
Tmx_dn	0.3201	-0.2263	0.03041	-0.2262	0.33159	-0.2471	-0.6341	5.89844
Tmn_up	-0.1866	0.1501	0.38555	0.1501	0.10759	-0.2555	-0.3402	5.29150
Tmn_dn	-1.8524	-0.1306	0.00000	0.9593	0.00008	-0.1745	0.3278	3.30773
Tmin_up	-1.1878	-0.0506	0.00000	0.7937	-0.00244	0.2601	-0.4382	1.94779
Tmin_dn	-0.5583	-0.1968	0.00000	0.5083	0.00332	-0.2254	0.3588	5.96784

Table 2.

The set of the fitting parameters corresponding to the GPD in accordance with expression (4b) for the integrated envelopes realized for the matrix (Q)

T(m)	ν_0	*Re*(ν_1)	/*Im*(ν_1)/	A_0	A_1	*RelErr(%)*
Tmx_up	0.78532	1.77386	0.00000	355.03579	-308.00920	0.22998
Tmx_dn	1.06733	1.06733	0.16232	-72.22792	1532.77121	0.23988
Tmn_up	1.08634	1.08634	0.15446	46.14889	-2292.03730	0.10587
Tmn_dn	0.86375	2.09519	0.00000	-392.98928	336.88393	0.22518
Tmin_up	0.94804	1.82027	0.00000	551.13572	-492.71538	0.10103
Tmin_dn	1.01502	1.17402	0.00000	-2175.86316	2096.73273	0.15680

Table 3.

The set of the fitting parameters corresponding to the GPD in accordance with expression (4a) realized for the matrix (U)

T(m)	ν_0	*Re*(ν_1)	/*Im*(ν_1)/	ν_2	A_0	A_1	A_2	*RelErr(%)*
Tmx_up	-1.2912	-0.1191	0.0000	0.7876	-0.00402	0.2475	-0.4594	3.53798
Tmx_dn	-0.5876	-0.0489	0.0000	0.4863	0.00031	-0.3785	0.5299	2.60659
Tmn_up	-1.6741	-0.2674	0.0000	0.9022	-0.00025	0.1193	-0.2869	6.87688
Tmn_dn	-0.6238	0.0592	0.0000	0.5301	-0.0001	-0.3822	0.5118	2.62642
Tmin_up	-0.7685	-0.0939	0.0000	0.6437	-0.45849	0.21197	-0.3418	2.42024
Tmin_dn	-0.8133	-0.2843	0.0000	0.5662	0.00035	-0.1221	0.2057	10.5272

Table 4.

The set of the fitting parameters corresponding to the GPD in accordance with expression (4b) for the integrated envelopes realized for the matrix (U)

T(m)	ν_0	*Re*(ν_1)	/*Im*(ν_1)/	A_0	A_1	*RelErr(%)*
Tmax_up	0.92082	1.64223	0.00000	671.65366	-606.66327	0.26253
Tmax_dn	1.00005	1.38469	0.00000	-1068.23467	976.33179	0.17450
Tmn_up	0.78202	1.76377	0.00000	384.18620	-359.34316	0.14900
Tmn_dn	1.02004	1.57326	0.00000	-627.89802	570.81066	0.12432
Tmin_up	0.92652	1.60321	0.00000	513.51494	-459.65031	0.17146
Tmin_dn	0.86399	1.29630	0.00000	-629.94090	554.29120	0.39902

The fitting parameters of the GPDs one can used for comparison of the CTs corresponding to two matrices (Q,U). The relative fitting error of the

cumulative/integrated fluctuations is more accurate (in ten times less) in comparison with fit of the initial envelopes.

S4. For demanded researchers, which want to understand deeper the nature of existing anisotropy it is important to compare the degree of correlations related to these irradiations. In order to evaluate these correlations, we use two types of independent expressions: (a) external correlations and (b) internal correlations based on the statistics of the fractional moments.

In the book of one of coauthors (RRN) [10] and in the papers [11, 12, 13] were shown how the statistics of the fractional moments (SFM) allows to evaluate external and internal correlations, which use for their calculation different expressions.

(a) External correlations for their evaluation use the following expression:

$$Cr_{l,m} = \frac{Range(s_i) + Range(s_l)}{Range(s_l, s_m)} \tag{6}$$

The Range(f) is determined by the second line of expression (5). This value is localized in the interval [0,2]. The interval [1,2] shows the interception degree (external correlations) for two compared sequences s_l and s_m, while the interval (0,1) shows the absence of external correlations.

(b) Internal correlations are evaluated in accordance with the following expressions:

$$GPCF_p = \frac{G_p(y_1, y_2)}{\sqrt{G_p(y_1, y_1) \cdot G_p(y_2, y_2)}},$$

$$G_p(y_1, y_2, \dots y_k) = \left(\frac{1}{N} \sum_{j=1}^{N} |yn_1(j) \dots yn_k(j)|^{mom_p} \right)^{\frac{1}{mom_p}}, \tag{7a}$$

$$yn(j) = \frac{y_j - min(y_j)}{max\left(y_j - min(y_j)\right)}, mom_p = exp\left(-r + 2\frac{p}{P}r\right),$$

$$exp(-r) \le mom_p \le exp(r), = 0,1, \dots, P.$$

The Generalized Pearson Correlation Function (GPCF) (7a) is localized in the interval [0,1] and as the relative measure of internal correlations one can take the following values of the complete correlations (CF)

$$CF(1) = M \cdot \left(\frac{Lim - M}{1 - M}\right), 0 \le CF(1) \le M, Lim = ln(mom_P), \tag{7b}$$

$$CF(2) = M \cdot Lim, M^2 \le CF(2) \le M.$$

Here *Lim* is the limiting value of the moment, which leads to the minimal correlations (reduced to the minimal value for CF(1), while the upper limit *M* associated with "remnant" correlations conserving the global minimum *M*, which always exist.

Based on these expressions one can evaluate the value of internal/external correlations and compare specific matrices (Q,U) that give the desired correlations

between the distributions (maxT(Q,U)), mnT(Q,U) and minT(Q,U) related to the selected CTs. The correlations evaluated in accordance with expressions (6) and (7) demonstrate clearly that external and internal correlations have *relative* character. From our point of view the problem with correlations is not completely solved and need the further research. Actually, one can pose the following question: is there the absolute value of correlations or in any specific case it is necessary to choose the relative values of correlations as it is shown in this small research. The values of correlations obtained in comparison of the CTs (Q) and (U) are shown in Tables 5 and 6.

Table 5.

External correlations between distributions associated with CTs. Minimal and maximal external correlations are bolded.

	maxT(Q)	*mnT(Q)*	*minT(Q)*
maxT(U)	1.7819	1.8011	**1.4951**
mnT(U)	1.7834	1.7642	1.8288
minT(U)	1.7079	1.6961	**1.9152**

Table 6.

Internal correlations that are evaluated in accordance with expressions (7b) The conventional Pearson correlation formula is added also for comparison all set of these internal correlations

	maxT(Q) CF(1)	*maxT(Q) CF(2)*	*maxT(Q) PCC*	*mnT(Q) CF(1)*	*mnT(Q) CF(2)*	*mnT(Q) PCC*	*minT(Q) CF(1)*	*minT(Q) CF(2)*	*minT(Q) PCC*
maxT(U)	0.0000	0.2123	0.8293	0.0094	0.2681	0.8203	0.1408	0.3943	0.8310
mnT(U)	0.0000	0.6147	0.8930	0.1797	0.6720	0.8881	0.0000	0.6167	0.9026
minT(U)	0.0000	0.4589	0.8868	0.2525	0.6509	0.8926	0.5666	0.8652	0.9414

Analysis of correlations from Table 6 shows that the CF(1) gives always lower correlations because that are counted relatively the value (1-*M*) in denominator, the CF(2) gives intermediate values, while the conventional Pearson correlation coefficient contains only higher values of correlations.

4. Conclusions

In this paper based on the obvious properties of the GPD we were able to describe quantitatively (Q) and (U) CMB polarization maps. Why the GPD(s) were turned out to be effective for description of these data belonging to random sequences not having clearly expressed trend? We want to underline here the following arguments: i) The GPD can replace in many cases "crude" language of histograms the power-law for more delicate "horizontal" distributions that are obtained by the splitting of the SRA for its positive and negative branches, correspondingly. ii) Why these branches (more sophisticated "histograms") have

the power-law behavior? Part of the arguments (based on the self-similarity principle) were given in paper [7]. Additional arguments were given in this paper. Combined arguments can be expressed mathematically by expressions (4). iii) How to apply the GPDs for real data? The algorithm was given in Section (3). The steps outlined in this section are rather general and can be applied to a wide class of the trendless sequences as well. iv) In addition to this tool as the GPDs one can add the statistics of the fractional moments. External and internal correlations give a possibility to compare the "vicinity" of different random sequences with each other from outside and inside as well.

REFERENCES

[1] *D.J. Fixsen*, The Temperature of the Cosmic Microwave Background, The Astrophysical Journal 707 (2), 916 (2009), arXiv:0911.1955.

[2] *M.J. Rees,* Polarization and spectrum of the primeval radiation in an anisotropic universe, The Astrophysical Journal 153, L1 (1968).

[3] *M.M. Basko, A.G. Polnarev*, Polarization and anisotropy of the RELICT radiation in an anisotropic universe, Mon. Not. R. Astrom. Soc. 191 (4), 207 (1980).

[4] *W. Hu, M. White*, A CMB polarization primer, New Astronomy 2, 323 (1997).

[5] *M. Kamionkowski, A. Kosowsky, A. Stebbins* , Statistics of cosmic microwave background polarization, Phys. Rev. D 55 (12), 7368 (1997).

[6] https://wiki.cosmos.esa.int/planckpla/index.php/CMB_and_astrophysical_component_map, [Online].

[7] *K.M. Gorsky et al,* HEALPix: A Framework for High-Resolution Discretization and Fast Analysis of Data Distributed on the Sphere, The Astrophysical Journal 622(2), 759 (2005).

[8] *R.R. Nigmatullin, D. Baleanu, O. Tintareanu, P. Stefanescu*, The Generalized Pareto Distribution: Its Applications to Cosmic Microwave Background, Rom. J. Phys. 69 (5-6), 403 (2024).

[9] *R.R. Nigmatullin*, Recognition of nonextensive statistic distribution by the eigen-coordinates method, Physica A, 285, 547 (2000).

[10] *R.R. Nigmatullin, P. Lino, G. Maione*, New Digital Signal Processing Methods Applications to Measurement and Diagnostics, ISBN 978-3-030-45359-6 (eBook), https://doi.org/10.1007/978-3-030-45359-6, Springer (2020).

[11] *R.R. Nigmatullin, A. Moroz, G. Smith*, Application of the Generalized Mean Value Function to the Statistical Detection of Water in Decane by Near-Infrared Spectroscopy, Physica A. 352, 379 (2005).

[12] *R.R. Nigmatullin*, Strongly Correlated Variables and Existence of the Universal Distribution Function for Relative Fluctuations, Phys. Wave Phenomena 16, 119 (2008).

[13] *R.R. Nigmatullin, P. Agarwal*, Direct evaluation of the desired correlations: Verification on real data, Physica A: Statistical Mechanics and its Applications 534, 121558 (2019).

[14] Planck Collaboration, Planck 2015 results I. Overview of products and scientific results, Astronomy & Astrophysics 594 (2016).